Theory of a ^{4}He parametric-resonance magnetometer based on atomic alignment

François Beato, Elie Belorizky, Etienne Labyt, Matthieu Le Prado, and Agustin Palacios-Laloy*
CEA-LETI, MINATEC Campus, F-38054 Grenoble, France
and Univ. Grenoble Alpes, F-38000 Grenoble, France

(Received 6 August 2018; published 26 November 2018)

In parametric-resonance magnetometers (PRMs), optically pumped atoms subject to rf fields allow one to measure the components of a very low magnetic field. Here, instead of using a circularly polarized light for creating atomic orientation, as in previous works, a linearly polarized light is used for creating atomic alignment. A dressed-atom formalism introduced by Polonsky and Cohen-Tannoudji is extended and allows one to map this situation to a simpler Hanle effect on aligned atoms. Analytical expressions for all alignment tensor components and photodetection signals are obtained for both the Hanle magnetometer and PRMs. A two-rf field alignment PRM is shown to display several improvements from its orientation counterpart, providing a secular third axis sensitivity and a lower degradation from the one-axis sensitivity obtained by using a single rf field. These specificities are shown to result from the apparent depolarization of the pumping light acting on the atom dressed by two-rf fields. Experimental measurements showing a good agreement with the theoretical predictions are presented.

DOI: 10.1103/PhysRevA.98.053431

I. INTRODUCTION

In the field of ultrasensitive magnetic measurements optically pumped magnetometers (OPMs) have reached excellent levels of accuracy [1–3] and sensitivities surpassing those of SQUIDs [4,5] without requiring cryogeny. Arrays of OPMs have been used for medical imaging of biological currents, which opens new perspectives notably in cardiography, fetal cardiography, and encephalography [6–8]. OPMs have also proved to be useful for improving the accuracy of fundamental measurements [9–11].

Between the various OPM configurations [12], Hanle magnetometers are particularly promising for medical imaging because they deliver real-time vector information on up to two components of the magnetic field [13]. These magnetometers operate at ambient fields sufficiently small so that relaxation rates are larger than Larmor frequencies.

An interesting variant is the so-called *parametric-resonance magnetometer* (PRM), which was pioneered by Dupont-Roc and his ENS Paris colleagues [13–15]. Based on the very same principles as Hanle magnetometers, but using a radio-frequency (rf) modulation, PRM avoids sensitivity to the $1/f$ noise of the probe beam, and has the advantage of providing a directional measurement along the rf field axis. PRM based on two rf allow real-time three-component measurement of the magnetic field [13,16].

Almost all the works on PRM rely on optical pumping of the atoms with circularly polarized light towards oriented states characterized by a non-null spin projection along one axis. However, using linearly polarized light it is possible to pump atoms with a spin larger than $1/2$ towards aligned states, defined by non-null second-order moments, like $3\langle S_z\rangle^2 - \langle \vec{S}^2\rangle \neq 0$.

Pumping with linearly polarized light has several advantages. First, in the case of circular polarization, there may be vector light shifts, equivalent to a virtual magnetic field, which cause various issues including field offsets, gradients, and increased noise [17]. In the case of linear polarization, there may be tensor light shifts, equivalent to a virtual quadrupole effect [18]. Secondly, the absence of a macroscopic magnetic moment of the atomic ensemble which could perturb the sensor environment. Thirdly, the possibility of easily controlling the pumping direction by rotating the polarization. In the case of scalar magnetometers this possibility allowed one to cancel the dead angles with an appropriate polarization-locking scheme [19,20]. There has been a renewed interest on alignment-based alkali-metal magnetometers these past years [21,22].

An interesting alternative to alkali metals is metastable ^{4}He, a spin-one which has been broadly used in scalar magnetometers [23,24] and more rarely in orientation-based PRM [25,26]. Recent medical trials have demonstrated the viability of a ^{4}He alignment-based PRM both for cardiography [27] and encephalography [28] with signals of typically 50 pT and 10 pT, respectively. In these two papers magnetometry signals have been successfully analyzed through the analytical expressions obtained in [16] for orientation-based PRM.

This article aims to provide a full description of the sensors used in these works and to provide an analytical treatment of alignment PRM in the same way as it was done for orientation [14–16].

We start (in Sec. II) by introducing the magnetometer setup. In Sec. III we introduce the formalism used to describe the atomic alignment with its evolution, and we compute the analytical expressions for the detection signals in two simple situations: Hanle effect with alignment and one-rf PRM.

*agustin.palacioslaloy@cea.fr

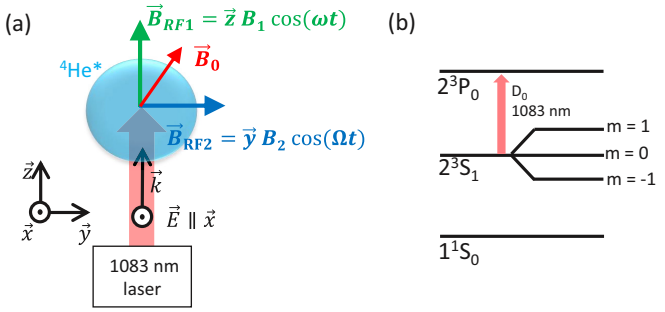

FIG. 1. (a) Setup of the alignment PRM: in order to measure $\vec{B}_0$, the metastable ^{4}He* atoms are enclosed in a glass cell, optically pumped by a linearly polarized light beam, with electrical field $\vec{E}$ along $\vec{x}$, and subject to two-rf fields. (b) Simplified spectrum of ^{4}He showing the three levels relevant for the magnetometer operation (not to scale); the metastable $2\,^3S_1$ level has three Zeeman sublevels characterized by $m = 0, \pm 1$.

Section IV introduces the dressed-atom formalism for aligned atoms. Section V discusses the application of this formalism to one- and two-rf PRM, allowing one to find analytical results under reasonable approximations. In Sec. VI we compare the theoretical predictions for two-rf PRM with preliminary experimental results. Finally, we conclude by discussing the specificities and advantages of alignment PRM.

II. OVERVIEW OF THE ALIGNMENT-BASED ^{4}He PARAMETRIC-RESONANCE MAGNETOMETER

Although the formalism presented here applies to any species which can be aligned, i.e., any spin $S > 1/2$, we will focus on ^{4}He in order to give a concrete description of an alignment-based PRM.

The relative position of the main elements of the magnetometer is sketched in Fig. 1. The sensitive element is contained in a glass cell: since ^{4}He ground $1\,^1S_0$ state has zero spin, we use the metastable $2\,^3S_1$ spin-one level. This level has three Zeeman sublevels characterized by their spin projection along a given direction $m = 1,\ 0,\ -1$. The populations of these sublevels can be prepared by optical pumping [29] using the upper $2\,^3P_x$ levels. For simplicity we will consider only D_0 $2\,^3S_1 \rightarrow 2\,^3P_0$ line. Metastable level cannot be optically populated. Therefore, a high-frequency (HF) discharge is used for this purpose. The discharge brings atoms from ground to high-energy states which quickly decay through a radiative cascade leaving a significant population only on the largest-lived state, the metastable level. Helium densities in this level up to 10^{12} cm^{-3} have been achieved even in relatively small cells [20].

PRM works in the low-field regime where the quasistatic field to be measured, of arbitrary direction, noted $\vec{B}_0 = B_x\vec{x} + B_y\vec{y} + B_z\vec{z}$, generates dynamics slower than the relaxation of the measuring atoms, i.e., $\gamma B_0 \ll \Gamma$, where γ is the gyromagnetic ratio of the sensitive species and Γ its relaxation rate. For ^{4}He $\gamma = -2\pi \times 28 \times 10^9$ rad/(s T) and typical $\Gamma \simeq 5$ kHz, yielding a limit of this low-field regime at $B_0 < 30$ nT.

Metastable relaxation on thermal ensembles is dominated by collisional processes because radiative decay to the ground state is doubly forbidden [30]. For helium enclosed in Torr-pressure cells at room-temperature collisional relaxation times are on the ms range, dominated by wall collisions and depolarizing collisions in the gas bulk, mainly three-body, Penning ionization and stepwise ionization [31–34].

In order to operate the PRM, two-rf fields are applied along the z and y axis orthogonal to the linear polarization of the pump, with angular frequencies ω and Ω larger than Γ, and sufficiently different. For instance in recent work [27] $\omega/2\pi = 40$ kHz and $\Omega/2\pi = 9$ kHz. The photodetection signal contains harmonics of ω and Ω as well as their interharmonics. It will be shown that some of these harmonics display a dispersive dependence with the magnetic-field components: the first harmonic of each rf is sensitive to the B_0 component parallel to the corresponding rf axis and their first interharmonic ($\omega \pm \Omega$) is sensitive to the third component of the magnetic field with lower sensitivity. In order to enlarge the dynamic range, PRM is usually operated in a closed-loop mode, where these three signals are sent to compensation coils which cancel the measured field locking to zero the three components of B_0 sensed by the atoms.

The distribution of metastable atoms inside the cell is far from being homogeneous and varies with the pressure and power of the discharge [20]. For the relatively low pressures used for magnetometry in 1 cm cells—typically 20 Torr—this distribution is very close to the first diffusion mode. This is in strong contrast with alkali metals in coated cells, where the walls are weakly depolarizing and the distribution is nearly homogeneous. In most of the calculations made below we have neglected this inhomogeneity by working on spatially averaged quantities. However, this approximation does not hold for evaluating the broadening of magnetic resonance lines by a magnetic-field gradient [35]. In this case the usual Robin contour condition used for weakly depolarizing walls should be replaced by a Dirichlet one, i.e., a null density of metastable atoms on the walls [36].

III. MATHEMATICAL DESCRIPTION OF THE SPIN ENSEMBLE AND ITS EVOLUTION

We analyze the magnetometer dynamics following the three-step approach [37]: (1) the system state is prepared by optical pumping, (2) this state evolves under the external magnetic field and the relaxation, and (3) the state is detected by optical measurements. Although the three processes are simultaneous in our system, this approach has been shown to remain valid in the low laser power limit [38,39], and has been successfully applied to other optically pumped magnetometers [21,22].

The state of the ensemble of metastable atoms can be represented by its 3×3 density matrix $\hat{\rho}$. The two first steps are described by the Liouville equation

$$\frac{d\hat{\rho}}{dt} = -i[\hat{H}(t), \hat{\rho}(t)] + \Gamma[\hat{\rho}_{ss} - \hat{\rho}(t)], \tag{1}$$

where $\hat{H}(t) = -\gamma \vec{B}_T(t) \cdot \vec{S}$ is the Zeeman Hamiltonian in angular frequency units, involving $\vec{B}_T(t) = \vec{x}B_{Tx} + \vec{y}B_{Ty} + \vec{z}B_{Tz}$, the total magnetic field including the static field $\vec{B}_0$ and the rf fields. The second term represents the optical pumping

and the relaxation, the combined effect of which tends to bring the system towards its steady state $\hat{\rho}_{ss}$ at a rate Γ. This total relaxation rate Γ is the combination $\Gamma_e + \Gamma_p$, where Γ_e is the relaxation of metastable atoms due to collisions and Γ_p is the state relaxation due to the optical pumping. A detailed analysis of the pumping with linearly polarized light [40] shows that with quantization axis parallel to pump polarization the steady-state density matrix $\hat{\rho}_{ss}$ is diagonal with $\rho_{00} = \Gamma_e/(3\Gamma_e + 3\Gamma_p)$ and $\rho_{11} = \rho_{-1-1} = (1 - \rho_{00})/2$.

In the case of spin one-half atoms the system evolution can be accurately described as the precession of a vector on the Bloch sphere. Spin-one atoms need a more complex description based on decomposition of the density matrix on the irreducible tensor operators (ITO) basis [41]:

$$\hat{\rho} = \sum_{k=0}^{2} \sum_{q=-k}^{+k} m_q^{(k)} \hat{T}_q^{(k)\dagger} = \sum_{k=0}^{2} \sum_{q=-k}^{+k} m_q^{(k)} (-1)^q \hat{T}_{-q}^{(k)}, \qquad (2)$$

where $m_q^{(k)} = \mathrm{Tr}(\hat{\rho}\hat{T}_q^{(k)})$ are the multipole moments which describe the spin polarization of the atomic ensemble and $\hat{T}_q^{(k)}$ are the $2k+1$ components of the ITO of order k. Order zero just describes the total state population and plays no role in magnetic measurement. Order 1 describes the *orientation*, with normalized vector components $(m_{-1}^{(1)}, m_0^{(1)}, m_1^{(1)}) = (\langle \hat{S}_- \rangle/2, \langle \hat{S}_z \rangle/\sqrt{2}, -\langle \hat{S}_+ \rangle/2)$. Order 2 describes the *alignment* tensor and can be represented as a column matrix M with elements $m_{-2}^{(2)}$, $m_{-1}^{(2)}$, $m_0^{(2)}$, $m_1^{(2)}$, $m_2^{(2)}$ [21,22]. ITOs have the following commuting relations with spin operators:

$$\begin{aligned} \left[\hat{S}_z,\ \hat{T}_q^{(k)}\right] &= q\hat{T}_q^{(k)}, \\ \left[\hat{S}_\pm,\ \hat{T}_q^{(k)}\right] &= \sqrt{(k \mp q)(k \pm q + 1)}\hat{T}_{q\pm1}^{(k)}. \end{aligned} \qquad (3)$$

Therefore, the Zeeman Hamiltonian induces no coupling between orders, notably between orientation and alignment. These couplings could appear for high pump powers if the laser is slightly detuned from the atomic transition: in this case a so-called *tensor lightshift* brings a Stark-like term in the Hamiltonian which induces alignment-to-orientation conversion [42]. Here, we will consider that the pump power is sufficiently low to avoid these effects. From Eq. (1) the time evolution of M takes a rather simple form:

$$\left[\frac{d}{dt} - \mathbb{H}(\vec{B}_T) + \Gamma\right] M = \Gamma M_{ss}. \qquad (4)$$

Steady-state alignment M_{ss} has components $\mathrm{Tr}(\hat{\rho}_{ss}\hat{T}_q^{(2)})$. The only non-null one is parallel to the pump polarization axis, and is written

$$m_{0,ss} = \frac{1}{\sqrt{6}} \frac{\Gamma_p}{\Gamma_p + \Gamma_e}. \qquad (5)$$

Thus choosing the quantization axis along $\vec{z}$, a pump linearly polarized along $\vec{x}$ yields a steady-state alignment M_{ss} with components $m_p(1, 0, -\sqrt{2/3}, 0, 1)$, where we have introduced $m_p = \Gamma_p/[4(\Gamma_p + \Gamma_e)]$. The Zeeman term is given by the matrix $\mathbb{H}(\vec{B}_T)$, where

$$\mathbb{H}(\vec{B}) = -i\gamma \begin{pmatrix} -2B_z & B_- & 0 & 0 & 0 \\ B_+ & -B_z & \sqrt{3/2}B_- & 0 & 0 \\ 0 & \sqrt{3/2}B_+ & 0 & \sqrt{3/2}B_- & 0 \\ 0 & 0 & \sqrt{3/2}B_+ & B_z & B_- \\ 0 & 0 & 0 & B_+ & 2B_z \end{pmatrix}, \qquad (6)$$

with $B_\pm = B_x \pm iB_y$. The matrix column M fully determines the detection signals. For instance, a probe linearly polarized along the x axis (which can be the pump beam itself) has an absorption coefficient which is written [43]

$$\kappa \propto \frac{m_0^{(0)}}{\sqrt{3}} + \frac{m_0^{(2)}}{\sqrt{6}} - \mathrm{Re}\left(m_2^{(2)}\right), \qquad (7)$$

the $m_q^{(k)}$ being expressed with z as quantization axis.

A. Hanle effect with transverse alignment pumping

A simple although interesting configuration to be analyzed with this formalism is the so-called alignment Hanle effect [22], corresponding to Fig. 1 without any rf field.

Let us consider first a rigorously null field: choosing the quantization axis along $\vec{z}$, a pump linearly polarized along $\vec{x}$ would yield M_{ss} with components $m_p(1, 0, -\sqrt{2/3}, 0, 1)$. Now if the pump light propagates along z and is partially depolarized, i.e., if its normalized Stokes parameters [44] are $S_1 = p < 1$, $S_2 = S_3 = 0$, p being the degree of polarization, the steady-state alignment M_{ss} components become $m_p(p, 0, -\sqrt{2/3}, 0, p)$.

Hanle effect manifests itself as a change in the steady state when a small magnetic field $|B_0| \ll \Gamma/\gamma$ is introduced. Equation (4) contains a constant Zeeman term dominated by the relaxation term. Its solution is an exponential decay in a time scale Γ^{-1} towards a steady state described by the analytical expressions given in Appendix A. These expressions being less compact than their orientation counterparts ([16, eq. I.4]), it is instructive to calculate the first-order terms in magnetic field:

$$\begin{aligned} m_2^{(2)}/m_p &\approx p\left(1 + 2i\frac{\omega_z}{\Gamma}\right) + O(\omega_i\omega_j), \\ m_1^{(2)}/m_p &\approx \left[\frac{\omega_y}{\Gamma}(p+1) + i(p-1)\frac{\omega_x}{\Gamma}\right] + O(\omega_i\omega_j), \\ m_0^{(2)}/m_p &\approx -\sqrt{2/3} + O(\omega_i\omega_j), \end{aligned} \qquad (8)$$

with $\omega_i = -\gamma B_i$ $(i = x,\ y,\ z)$.

Using Eq. (A1), Fig. 2 shows how the degree of polarization influences the dependence of $m_q^{(2)}$ on the components of the magnetic field. When the pump is fully polarized ($p = 1$, solid line) the alignment only varies with z and y components of B_0, exactly like the case of orientation-based Hanle effect. However, when the pump is partially depolarized ($0 < p < 1$, dashed lines) information about the three axes is contained in M. However, it is not easy to find a probing scheme able to recover it. As we will show below, two-rf PRM provides one of such schemes.

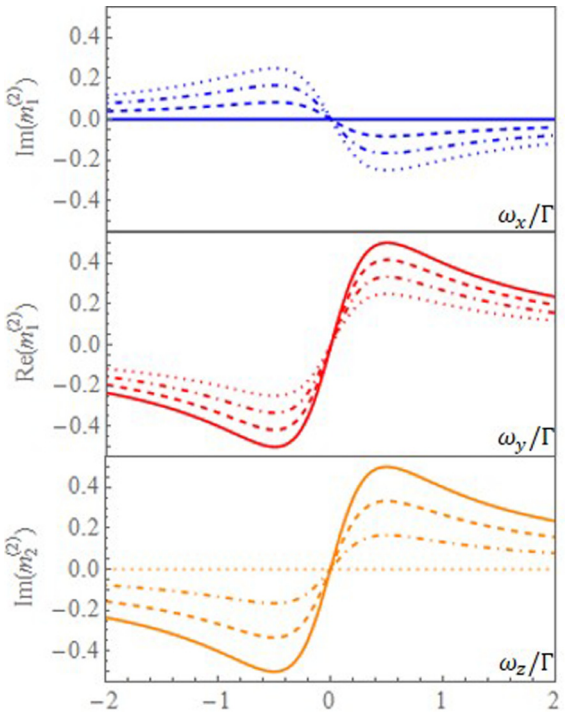

FIG. 2. Dependence of $m_q^{(2)}$ on the magnetic-field components calculated from Eq. (A1). The degree of polarization is represented by solid lines ($p = 1$) and dotted lines: p decreasing from 2/3 to zero by steps of 1/3. (Top) Dependence of $\mathrm{Im}(m_1^{(2)})$ on ω_x (assuming $\omega_y = \omega_z = 0$). (Middle) Dependence of $\mathrm{Re}(m_1^{(2)})$ on ω_y (assuming $\omega_x = \omega_z = 0$). (Bottom) Dependence of $\mathrm{Im}(m_2^{(2)})$ on ω_z (assuming $\omega_x = \omega_y = 0$).

B. Single-rf parametric-resonance magnetometer with B_0 parallel to the rf field

When the magnetic field has an oscillating component, the system does not evolve anymore towards a steady state. However, when the dc and oscillating parts of the magnetic field are parallel, it is possible to find an analytic solution for M. Indeed the evolution matrix $\mathbb{H}(\vec{B}) = \mathbb{H}(\vec{z}[B_0 + B_1\cos(\omega t)])$ is diagonal, allowing the decoupling of the five equations describing the evolution of M. With pump polarization along x (i.e., setup of Fig. 1 without B_{rf2}) the components of M_{ss} are $m_p(1, 0, -\sqrt{2/3}, 0, 1)$ and the only nontrivial equations read

$$\dot{m}_{\pm 2}^{(2)} = \mp i\gamma 2[B_0 + B_1\cos(\omega t)]m_{\pm 2}^{(2)} - \Gamma\left(m_{\pm 2}^{(2)} - m_p\right). \quad (9)$$

These equations are formally equivalent to those given for orientation in [14, Eq. (15a)]. The solutions are

$$m_{\pm 2}^{(2)} = \Gamma m_p \sum_{n,p=-\infty}^{+\infty} \frac{J_{n,2}J_{n-p,2}}{\Gamma \pm i(2\gamma B_0 + n\omega)} e^{\pm ip\omega t}, \quad (10)$$

with $J_{n,s} = J_n(s\gamma B_1/\omega)$ and J_n the Bessel function of the first kind and order n. When probing with the pump beam itself Eq. (7) gives the pump absorption. The photodetector signal has a component at frequency ω, corresponding to $n = 0$, $p = \pm 1$, which is in quadrature with the rf field and is given by

$$-4\Gamma m_p J_{0,2}J_{1,2}\frac{\gamma B_0}{\Gamma^2 + 4\gamma^2 B_0^2}\sin(\omega t). \quad (11)$$

This expression is very similar to that appearing for orientation PRM [14, Eq. (31)], except for the arguments of Bessel functions and numerical prefactors, and it can be also used for measuring the field B_0.

IV. DRESSED-ATOM FORMALISM FOR ALIGNMENT

Up to now we have considered simple situations where analytical results are easy to obtain. More complex cases, like the introduction of a second rf, strongly benefit from the introduction of the dressed-atom formalism. In this formalism the time dependence of the Hamiltonian is avoided with a quantum treatment of the rf field. This formalism has been applied to oriented atoms [16,45–47] and was extended to all tensor orders in [47]. Here, we will develop the case of aligned atoms with an arbitrarily oriented external field $\vec{B}_0$. We will show, like it was done for orientation in [16], that it allows one to map the PRM to a simpler Hanle-effect problem, unveiling physical effects which otherwise remain hidden in complicated analytical or numerical solutions.

A. Null-field Hamiltonian and its eigenstates

Let us note $|m\rangle$ the metastable ^{4}He $\hat{S}_z$ eigenstates ($m = -1, 0, 1$). In the absence of any static magnetic field the Hamiltonian describing this atom and the rf field $\vec{B}_{rf1}$ with linear polarization along z is

$$\hat{H}_0 = \omega\hat{a}^\dagger\hat{a} + \lambda\hat{S}_z(\hat{a}^\dagger + \hat{a}), \quad (12)$$

where the field is described with Fock states $|n\rangle$ and creation and annihilation photon operators $\hat{a}^\dagger$ and $\hat{a}$. The coupling constant is proportional to the amplitude of the rf through $\lambda = -\gamma B_1/(2\sqrt{\bar{n}})$, where the average photon number is $\bar{n} = \langle\hat{a}^\dagger\hat{a}\rangle$. The eigenstates of H_0 can be found [16,48] to be $|m\rangle \otimes |n_m\rangle$ where $|n_m\rangle = \hat{D}(m\lambda/\omega)|n\rangle$, with displacement operator $\hat{D}(\alpha) = \exp[\alpha(\hat{a} - \hat{a}^\dagger)]$. An important property of these eigenstates is $\langle n_m|n'_{m'}\rangle = J_{n-n'}[(m - m')\gamma B_1/\omega]$ for $n \gg 1$. In what follows, for shortening the notation, we define

$$J_{p,q} = J_p[q\gamma B_1/\omega]. \quad (13)$$

B. Evolution of the observables of the dressed atom: Effect of a static external field

We now add the static magnetic field $\vec{B}_0$ of small magnitude ($\gamma B_0 \ll \Gamma$, γB_1) as a perturbation $\hat{V} = -\gamma\vec{B}_0\cdot\vec{\hat{S}} = -\gamma(B_x\hat{S}_x + B_y\hat{S}_y + B_z\hat{S}_z)$. In order to analyze the effect of this term for each rf photon number we introduce the projection operator $\hat{P}_n = \sum_m |m, n_m\rangle\langle m, n_m|$ and the projected operators ${}^{n,n'}\hat{X} = \hat{P}_n\hat{X}\hat{P}_{n'}$. The evolution equation of the projected operators ${}^{n,n'}\hat{T}_q^{(2)}$ due to $\hat{H}_0 + \hat{V}$ is

$$\frac{d}{dt}{}^{n,n'}\hat{T}_q^{(2)} = -i\left[{}^{n,n'}\hat{T}_q^{(2)}, \hat{H}_0 + \hat{V}\right]. \quad (14)$$

The null-field Hamiltonian can be written $\hat{H}_0 = \sum_n n\omega\hat{P}_n$ and each ${}^{n,n'}\hat{T}_q^{(2)}$ evolves at an eigenfrequency $(n - n')\omega$. The perturbation brings $[{}^{n,n'}\hat{T}_q^{(2)}, \hat{S}_i]$ terms which do not satisfy the usual relations (3). Indeed the matrix elements of the projected

ITOs are

$$\langle m, n_m|^{n,n'}\hat{T}_q^{(2)}|m', n'_{m'}\rangle = \langle m|\hat{T}_q^{(2)}|m-q\rangle J_{n-n',q}\delta_{m',m-q}. \quad (15)$$

Therefore, $[\hat{S}_i, {}^{n,n'}\hat{T}_q^{(2)}]$ contains Bessel terms which depend on $n-n'$. In order to avoid this dependence, it is convenient to work with dressed-atom ITO (DITO) ${}^{n,n'}\tilde{\mathcal{T}}_q^{(2)}$ operators defined by

$${}^{n,n'}\tilde{\mathcal{T}}_q^{(2)} = \frac{{}^{n,n'}\hat{T}_q^{(2)}}{J_{n-n',q}}. \quad (16)$$

These DITO have the usual commuting relations (3) with dressed spin operators defined in the same way:

$${}^{n,n'}\tilde{\mathcal{S}}_q^{(2)} = \frac{{}^{n,n'}\hat{S}_q^{(2)}}{J_{n-n',q}}. \quad (17)$$

To suppress also the dependence with n coming from $\hat{H}_0$, DITO can be written in the interaction picture:

$${}^{n,n'}\tilde{\mathcal{T}}_q^{(2)} = {}^{n,n'}\tilde{\mathcal{T}}_q^{(2)}e^{-i\omega(n-n')t}. \quad (18)$$

Then, neglecting all the nonsecular terms (${}^{l,l'}V$ with $l' \neq l$), the evolution of ${}^{n,n'}\tilde{\mathcal{T}}_q^{(2)}$ under the magnetic field is written simply

$$\frac{d}{dt}^{(1)}\left\langle {}^{n,n'}\tilde{\mathcal{T}}_q^{(2)}\right\rangle = \mathbb{H}(\bar{B}_0)\left\langle {}^{n,n'}\tilde{\mathcal{T}}_q^{(2)}\right\rangle, \quad (19)$$

where $\mathbb{H}$ is given by Eq. (6); $\bar{B}_0$ is defined from $\vec{B}_0$ by the affinity

$$\bar{B}_{x,y} = J_{0,1}B_{x,y}, \quad \bar{B}_z = B_z, \quad (20)$$

when the rf direction is along $\vec{z}$. In what follows we will use $\bar{\omega}_i = -\gamma\bar{B}_i$ $(i = x, y, z)$. Equation (19) shows that in the dressed-atom picture the Zeeman term is time independent, strongly simplifying the description of the PRM dynamics.

C. Effect of relaxation and optical pumping on the evolution of dressed-atom observables

The description of PRM dynamics in the dressed-atom picture requires two other terms—describing relaxation and optical pumping, respectively. For ^{4}He, relaxation is dominated by collisional isotropic processes. Thus the relaxation term is simply written

$$\frac{d}{dt}^{(2)}\left\langle {}^{n,n'}\tilde{\mathcal{T}}_q^{(2)}\right\rangle = -\Gamma\left\langle {}^{n,n'}\tilde{\mathcal{T}}_q^{(2)}\right\rangle. \quad (21)$$

On other systems, where relaxation involves anisotropic phenomena, three relaxation rates $\Gamma_{|q|}$ are needed [49].

The optical pumping term has been calculated in [45] and is written

$$\frac{d}{dt}^{(3)}\frac{\left\langle {}^{n,n'}\hat{T}_q^{(2)}\right\rangle}{p(n)} = \Gamma_p\, m_{q,ex}\, e^{i(n-n')\omega t}\, e^{-iq\gamma B_1 \sin(\omega t)/\omega} J_{n-n',q}, \quad (22)$$

with $p(n)$ the probability of having n photons in the coherent rf fields and $\Gamma_p\, m_{q,ex} = \Gamma\, m_{q,ss}$. Introducing the DITO defined by Eq. (16), and applying the Jacobi-Anger expansion Eq. (B1) to the term depending on B_1 on the above expression, we get

$$\frac{d}{dt}^{(3)}\frac{\left\langle {}^{n,n'}\tilde{\mathcal{T}}_q^{(2)}\right\rangle}{p(n)} \approx \Gamma\, J_{0,q}\, m_{q,ss}, \quad (23)$$

where we have kept only the secular term, which is static in the dressed-atom picture and evolves at frequency $(n-n')\omega$ in the laboratory frame. This result corresponds to a rescaling of the pumping term M_{ss} to a *dressed-pumping* $\bar{M}_{ss}$ with components:

$$\bar{m}_{q,ss} = J_{0,q}\, m_{q,ss}. \quad (24)$$

D. Solution of the evolution equation

Combining the three evolution terms we get for the dressed atom:

$$\left[\frac{d}{dt} - \mathbb{H}(\bar{B}_0) + \Gamma\right]\frac{\left\langle {}^{n,n'}\tilde{\mathcal{T}}_q^{(2)}\right\rangle}{p(n)} = \Gamma\,\bar{m}_{q,ss}. \quad (25)$$

This equation is formally identical to Eq. (4) relative to the Hanle effect on the naked atom. Thus the analytical solutions for $\bar{m}_q^{(2)} = \langle {}^{n,n'}\tilde{\mathcal{T}}_q^{(2)}\rangle/p(n)$ are those given in (A1). The evolution of the ITO $\langle\hat{T}_q^{(2)}\rangle$ in the laboratory frame is obtained from the evolution of the DITO $\bar{m}_q^{(2)}$ by applying Eq. (16):

$$\left\langle\hat{T}_q^{(2)}\right\rangle = \sum_{n,n'} J_{n-n',q}e^{i(n-n')\omega t}\, p(n)\bar{m}_q^{(2)} \approx \bar{m}_q^{(2)}\exp\left(iq\frac{\gamma B_1}{\omega}\sin(\omega t)\right), \quad (26)$$

where we have used the approximation [16]

$$\sum_{n,n'} J_{n-n',q}e^{i(n-n')\omega t}\, p(n) \approx \exp\left(iq\frac{\gamma B_1}{\omega}\sin(\omega t)\right), \quad (27)$$

which is valid for $\bar{n} \gg 1$ as explained in [45,48].

E. Summary of the dressed-atom formalism applied to PRM

The dressed-atom formalism allows one to map the PRM problem to the much simpler Hanle effect, the solutions of which have been found above [Eq. (A1)]. This mapping is done by (i) rescaling the magnetic field as described by the affinity (20) and (ii) modifying the pumping term as given by (24).

Once the solution has been found in this dressed-atom picture, a rotation by an angle $\gamma B_1 \sin(\omega t)/\omega$ around the rf axis [Eq. (26)] directly yields the solution in the laboratory frame.

This solution involves only the following two approximations.

(i) The presence of a sufficiently large number of rf photons $\bar{n} \gg 1$, which is always true for the classical rf field of PRM.

(ii) The secular approximation $\omega \gg \gamma B_0$, Γ, which is a more restrictive condition. The first-order nonsecular corrections can be calculated for alignment in a similar way to that given for orientation in the appendix of [16]. They will be published elsewhere.

V. PARAMETRIC-RESONANCE MAGNETOMETER STUDY IN THE DRESSED-ATOM FORMALISM

A. Single-rf parametric-resonance magnetometer with B_0 parallel to the rf field

Although we have seen that this situation is analytically solvable without the dressed-atom formalism, it gives a first example of application. The pumping steady-state M_{ss}components are $m_p(J_{0,2}, 0, -\sqrt{2/3}, 0, J_{0,2})$, which correspond to a partially polarized pumping beam with a degree of polarization $p = J_{0,2}$. Using (26), (8), and the Jacobi-Anger expansion [50], we get a constant $m_0^{(2)}$ and

$$\begin{aligned} m_2^{(2)} &= \bar{m}_2^{(2)} e^{i2\frac{\gamma B_1}{\omega}\sin(\omega t)} \\ &= m_p p\left(1 + 2i\frac{\bar{\omega}_z}{\Gamma}\right)\sum_{q=-\infty}^{\infty} J_{q,2} e^{iq\omega t}. \end{aligned} \tag{28}$$

The absorption coefficient for the pump can be found from Eq. (7). Since $\bar{\omega}_z = \omega_z$ and $p = J_{0,2}$ it contains a single component at ω which is written $-4m_p J_{0,2} J_{1,2} \sin(\omega t)\omega_z/\Gamma$, in agreement with the linear part of Eq. (11).

B. Double-rf parametric-resonance magnetometer

In the case of a double-rf PRM direct analytical solutions are hardly tractable and difficult to be interpreted. The dressed-atom formalism provides a convenient way to address this situation. Indeed we can first dress the atom with the faster rf field, of angular frequency ω, while considering the slower one as quasistatic, and then dress the atom with the second slower rf field of angular frequency Ω. After these two dressings, the rf fields have been traced out and the dynamics of the atom reduces to a Hanle-effect problem.

From Eq. (24), this double dressing of the pumping yields

$$\begin{aligned} \bar{\bar{m}}_{2,ss} &= -\frac{m_p}{2}(J_{0,2} + 1)\mathscr{J}_{0,2}, \\ \bar{\bar{m}}_{1,ss} &= 0, \quad \bar{\bar{m}}_{0,ss} = \frac{m_p}{\sqrt{6}}(1 - 3J_{0,2}), \end{aligned} \tag{29}$$

with $J_{n,q} = J_n(q\gamma B_1/\omega)$ and $\mathscr{J}_{n,q} = J_n(q\gamma \bar{B}_2/\Omega) = J_n(q\gamma J_{0,1} B_2/\Omega)$. Thus the double dressing has the following two effects on the pumping.

(i) An overall reduction of the pumping amplitude $m_p \to -m_p(1 - 3J_{0,2})/2$.

(ii) A variation of $\bar{\bar{m}}_{\pm 2,ss}$ as compared to $\bar{\bar{m}}_{0,ss}$, which can be interpreted as a partial depolarization of the pumping light by comparison with the undressed pumping term (M_{ss} given in Sec. II). A pure linear polarization is described by a degree of polarization $p = 1$; the dressing reduces it to a value

$$p = -\mathscr{J}_{0,2}(1 + J_{0,2})/(1 - 3J_{0,2}). \tag{30}$$

The effective magnetic field acting on the dressed atom is found using twice the affinity (20):

$$\bar{\bar{B}}_x = B_x J_{0,1}\mathscr{J}_{0,1}, \quad \bar{\bar{B}}_y = B_y J_{0,1}, \quad \bar{\bar{B}}_z = B_z \mathscr{J}_{0,1}. \tag{31}$$

Therefore, the doubly dressed atom has the following Hanle effect solution, calculated to first order in each magnetic-field component:

$$\begin{aligned} \bar{\bar{m}}_2 &= -\frac{m_p}{2}\mathscr{J}_{0,2}(1 + J_{0,2})\left(1 + i2\frac{\omega_y}{\Gamma}J_{0,1}\right), \\ \bar{\bar{m}}_1 &= -\frac{m_p}{2}\mathscr{J}_{0,1}\Big[\frac{\omega_x}{\Gamma}J_{0,1}(\mathscr{J}_{0,2} + \mathscr{J}_{0,2}J_{0,2} + 1 - 3J_{0,2}) \\ &\quad + i\frac{\omega_z}{\Gamma}(\mathscr{J}_{0,2} + \mathscr{J}_{0,2}J_{0,2} - 1 + 3J_{0,2})\Big], \\ \bar{\bar{m}}_0 &= m_p(1 - 3J_{0,2})/\sqrt{6}. \end{aligned} \tag{32}$$

The signals in the laboratory frame can be obtained from these dressed-atom picture solutions by using Eq. (26). The absorption coefficient Eq. (7) is written

$$\begin{aligned} \kappa \propto\ & \bar{\bar{m}}_0\left(\frac{1}{\sqrt{6}} - \sqrt{\frac{3}{2}}c_{2,\omega}\right) + 2\,\mathrm{Im}(\bar{\bar{m}}_1)s_{2,\omega}\bar{c}_{1,\Omega} \\ & + 2\,\mathrm{Re}(\bar{\bar{m}}_1)s_{2,\omega}\bar{s}_{1,\Omega} + \mathrm{Im}(\bar{\bar{m}}_2)[c_{2,\omega} + 1]\bar{s}_{2,\Omega} \\ & - \mathrm{Re}(\bar{\bar{m}}_2)[1 + c_{2,\omega}]\bar{c}_{2,\Omega}, \end{aligned} \tag{33}$$

with $c_{p,\omega} = \cos[p\gamma B_1 \sin(\omega t)/\omega]$ and $\bar{c}_{p,\Omega} = \cos[p\gamma \bar{B}_2 \sin(\Omega t)/\Omega] = \cos[p\gamma B_2 J_{0,1} \sin(\Omega t)/\Omega]$, $s_{p,\omega}$ and $\bar{s}_{p,\Omega}$ the corresponding expressions with sines instead of cosines. Combining Eqs. (32) and (33), and using the Jacobi-Anger expansions Eqs. (B1) of $c_{p,\omega}$, $s_{p,\omega}$, $\bar{c}_{p,\Omega}$, and $\bar{s}_{p,\Omega}$, first-order dependence on each magnetic-field component appears at different frequencies in κ as follows.

(i) Components at frequencies $2n\omega \pm (2m + 1)\Omega$ with $m, n = 0, 1, \ldots$ arising from the fourth term in Eq. (33) are proportional to B_y. The component at frequency Ω has an amplitude

$$m_p \mathscr{J}_{0,2}\mathscr{J}_{1,2}J_{0,1}(1 + J_{0,2})^2\frac{\omega_y}{\Gamma} = s_y\frac{\omega_y}{\Gamma} \tag{34}$$

allowing the measurement of the field along the axis of rf_2.

(ii) Components at frequencies $(2n + 1)\omega \pm 2m\Omega$, arising from the second term of Eq. (33), are proportional to B_z. The component at frequency ω has an amplitude

$$m_p \mathscr{J}_{0,1}^2 J_{1,2}[\mathscr{J}_{0,2}(1 + J_{0,2}) - 1 + 3J_{0,2}]\frac{\omega_z}{\Gamma} = s_z\frac{\omega_z}{\Gamma} \tag{35}$$

and allows the measurement of the field along the axis of rf_1.

(iii) Components at frequencies $(2n + 1)\omega \pm (2m + 1)\Omega$, arising from the third term of Eq. (33), are proportional to B_x. The first component is at frequency $\omega + \Omega$ with an amplitude

$$\begin{aligned} & m_p \mathscr{J}_{1,1}J_{1,2}\mathscr{J}_{0,1}J_{0,1} \\ & \quad \times[\mathscr{J}_{0,2}(1 + J_{0,2}) + 1 - 3J_{0,2}]\omega_x/\Gamma = s_x\omega_x/\Gamma, \end{aligned} \tag{36}$$

allowing the measurement of the field along the pump polarization axis. Note that these terms would cancel if $p = 1$, i.e.,

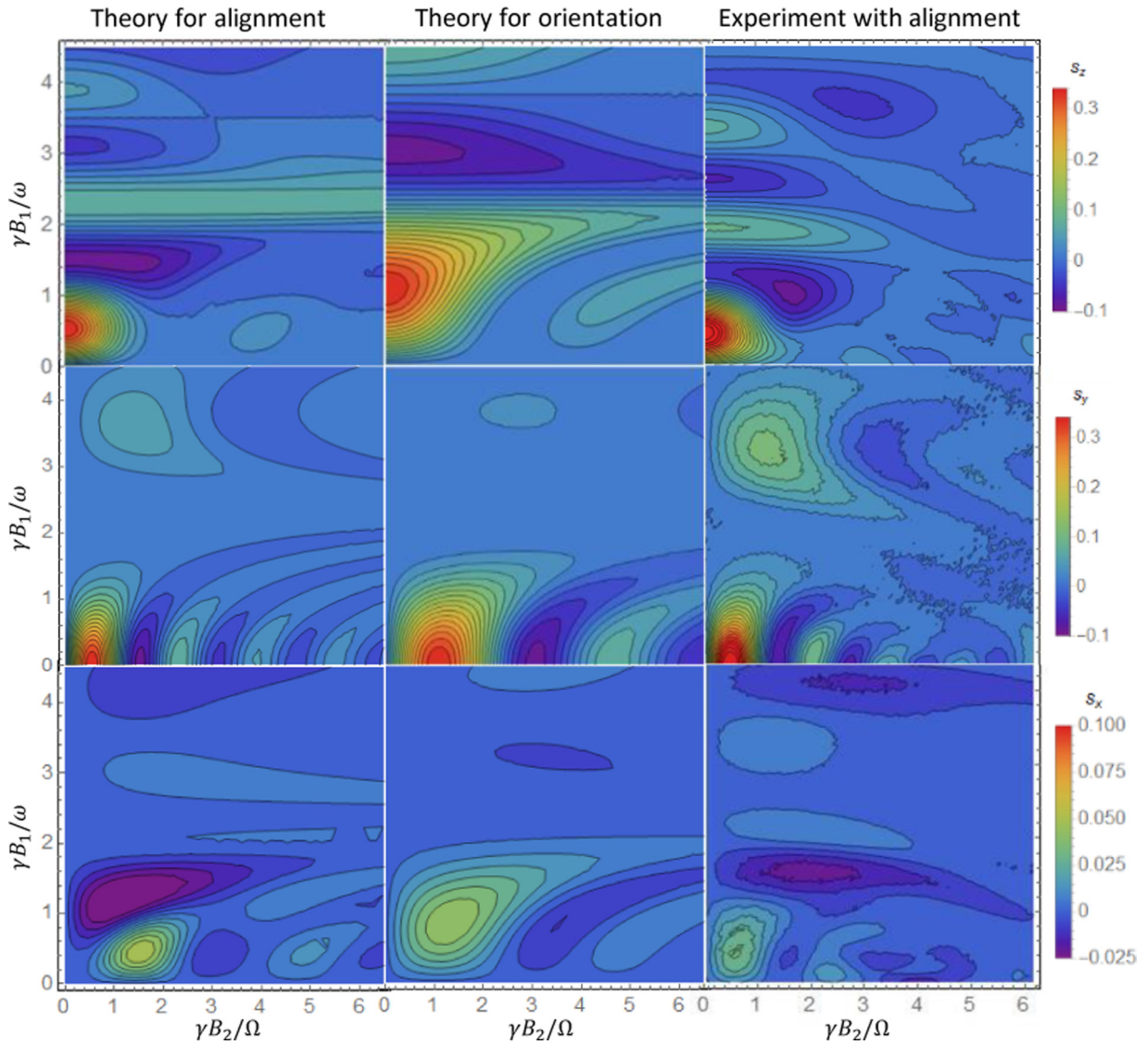

FIG. 3. Left column: theoretical sensitivities s_x, s_y, s_z of alignment-based two-rf PRMs defined by Eqs. (34)–(36) as functions of the rf field amplitudes. Center column: theoretical sensitivities for orientation-based two-rf PRMs as given by [16]. For both columns we set $m_p = 1/4$. Right column: experimental characterization of the sensitivities of a two-rf ^{4}He PRM pumped with linearly polarized light as a function of the rf field amplitudes. See the text for a description of the setup. Experimental sensitivities are normalized by the ratio between the observed highest z-axis sensitivity and its theoretical value.

if the pumping was not partially depolarized by the dressing [Eq. (30)].

(iv) All other components at frequencies $2n\omega$, $2m\Omega$, and $2n\omega \pm 2m\Omega$ show no first-order dependence on the magnetic field.

In Eqs. (34)–(36) we have introduced the magnetic-field sensitivities s_x, s_y, and s_z. These sensitivities are plotted as a function of B_1 and B_2 and compared to their orientation-PRM counterparts [13] on Fig. 3. Note that for orientation-based PRM the theoretical sensitivity along x axis is null with the secular approximation. Then, the plot represents s_x obtained from the first-order nonsecular correction for $\Omega = 2\Gamma$.

Both for orientation and alignment, the optimal sensitivity of the z and y axes is reached when the rf field of the other axis is turned off. In this one-rf scheme the optimal values of $\gamma B_2/\Omega$ and $\gamma B_1/\omega$ for alignment are half of those for orientation. When the two rf are present, even if there are some similarities between alignment and orientation, the respective sensitivities show a very different behavior.

When operating this PRM as a two-axis magnetometer it is usual to seek the best possible sensitivity for both z and y axes. This optimum corresponds to the maximum of $s_2 = (s_y^2 + s_z^2)^{1/2}$, under the condition of keeping similar sensitivities along both axes. These optima are shown in Fig. 4 for alignment and orientation. For orientation PRMs the optimum is at a saddle point. The corresponding sensitivities s_y and s_z display a degradation of 37% with respect to their maximal value for single-rf PRMs. For alignment PRMs s_2 reaches a higher value, and this maximum is located on the

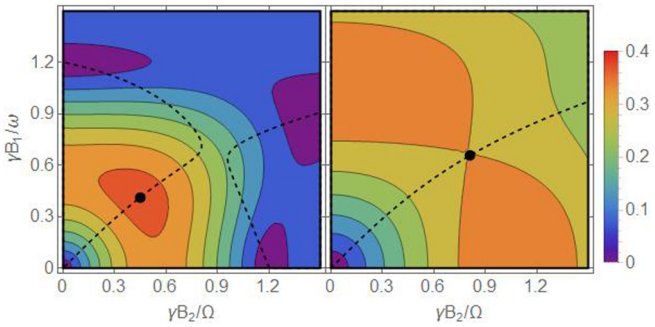

FIG. 4. Two-axis sensitivity $s_2 = \sqrt{s_y^2 + s_z^2}$, as a function of the rf field amplitudes, for alignment (left) and orientation (right) PRMs. The dashed lines represent isosensitivity ($s_y = s_z$). The black disk represents the maximal isosensitivity.

isosensitivity curve. The corresponding sensitivities s_y, s_z display a degradation of only 23% with respect to their maximal value for single-rf PRMs.

VI. PRELIMINARY EXPERIMENTAL CHARACTERIZATIONS

In order to probe the above theoretical predictions, we compared them to the experimental sensitivities measured on a ^{4}He alignment-based parametric-resonance magnetometer.

The experimental setup consists in a cylindrical pyrex cell of 1 cm $\oslash \times 1$ cm internal dimensions, filled with 20 Torr of high purity ^{4}He, and placed at the center of three-axes square coils of 39 cm side. All these elements are set inside a five-layer μ-metal magnetic shielding. The helium metastable level is populated by using an HF discharge through square copper electrodes glued on the cell wall. A laser beam is sent through the cell, with its linear polarization parallel to the x axis coil, a waist of 6 mm, and a power around 50 μW. This laser is tuned to the absorption line D_0 of helium. The laser beam is photodetected by InGaAs photodiode connected to a transimpedance amplifier. The two-rf fields are generated by a two-channel signal generator directly connected to the coil inputs. Careful calibration of coil impedance and transfer functions allow one to translate the generator voltages to rf magnetic field units. The frequencies of the rf fields were chosen to be $\Omega/2\pi = 7$ kHz for y axis and $\omega/2\pi = 25$ kHz for z axis.

For measuring the sensitivities of z and y axis a slow ramp in the field of 2 s is applied and the photodetection signal is sent to a digital lock-in (Stanford 865A). A LabView program acquires the signals at lock-in output and fits their slope. We characterized with an automated procedure the sensitivities of the three axis for 11680 pairs of rf values. These sensitivities are presented in Fig. 3.

The measured sensitivities are completely different from those predicted for orientation (center column of Fig. 3), and are rather similar to those predicted for alignment (left column of Fig. 3). The z- and y-axes sensitivities show a very good agreement with predictions: the position and shape of the optimal sensitivity region (obtained at $\gamma B_1/\omega$ and $\gamma B_2/\Omega$ values of 0.541) and most of the other features are well matched. However, few discrepancies appear: the features in the $\gamma B_1/\omega > 2$ region appear at lower values than those predicted by the theory. Some other features, like the variation of s_z vs B_2 which is predicted to be constant for $\gamma B_1/\omega \approx 2$ shows a progressive decrease with increasing B_2. The x-axis sensitivity shows a fair agreement with the predictions although not as good as for the two other axes. Some disagreements appear for low rf ($\gamma B_1/\omega$, $\gamma B_2/\Omega < 1$): the optimal sensitivity is reached at a B_2 value lower than expected and the negative-sensitivity region starts at B_1 values larger than predicted.

The disagreements in z- and y-axes sensitivities could arise from coil inhomogeneity which generates significant rf gradients for large rf field amplitude [51]. We also suspect that the rf could also induce Eddy currents in the electrodes. In similar experiments [47] such currents are reported to bring a few percent of circular polarization to the rf field, which distort the resonances. Overall, we can conclude that these preliminary experimental characterizations are in rather good agreement with the theoretical predictions made above.

VII. CONCLUSION

In this article we have studied a two-rf alignment-based PRM which is able to provide three-axes measurement of the ambient magnetic field. We have found analytical expressions for its photodetection signals by using the dressed-atom formalism. These expressions yield sensitivities which are in good agreement with preliminary experimental characterizations.

This analysis highlights some interesting advantages of alignment-based PRM in addition to the suppression of vector light shifts. In particular, we have shown that in the case of two-rf PRM a secular term allows the measurement of the third component of the magnetic field. Moreover, s_y, s_z sensitivities present a lower degradation with respect to the single-axis sensitivity. We believe that alignment-based PRM is a promising configuration for implementing vector optically pumped magnetometers, as suggested by the measurements of biomagnetic signals [27,28].

By mapping the two-rf PRM to a Hanle effect problem, the dressed-atom formalism sheds some light on the underlying mechanisms. In particular, it appears that the third-axis sensitivity results from the apparent depolarization of the pump light acting on the doubly dressed atom [Eq. (30)]. This is in strong contrast with the case of orientation-based PRM where this dressing only reduces the pump amplitude.

Our analysis also suggests that partial depolarization could be combined with polarization rotation [19,20] to yield interesting magnetometry schemes.

ACKNOWLEDGMENTS

We acknowledge W. Fourcault for the design and fabrication of the experimental setup, F. Alcouffe for cell fabrication, S. Morales, T. Jager, F. Bertrand, and J. M. Léger for interesting discussions, and financial support from H2020-ICT-2014-1 gateone project and Carnot CEA-LETI.

APPENDIX A: HANLE EFFECT ALIGNMENTS UNDER PARTIALLY LINEARLY POLARIZED TRANSVERSE PUMPING

Starting from Eq. (4), for the steady state, after a matrix inversion, one finds

$$\frac{m_0^{(2)}}{m_p} = -\sqrt{\frac{2}{3}}\frac{\Gamma^4+\Gamma^2\left[(3p+2)\omega_x^2+(2-3p)\omega_y^2+5\omega_z^2\right]+18\Gamma p\omega_x\omega_y\omega_z+\left(\omega_x^2+\omega_y^2-2\omega_z^2\right)\left[(3p+1)\omega_x^2+(1-3p)\omega_y^2-2\omega_z^2\right]}{\Delta},$$

$$\frac{m_1^{(2)}}{m_p} = \frac{\Gamma^3[(p+1)\omega_y+i(p-1)\omega_x]+\Gamma^2\omega_z[(1-3p)\omega_x+i(1+3p)\omega_y]-2\omega_z(\omega_x+i\omega_y)\left[(3p+1)\omega_x^2+(1-3p)\omega_y^2-2\omega_z^2\right]}{\Delta}$$
$$+\frac{\Gamma i(p-1)\omega_x^3+(7p+1)\omega_x^2\omega_y+i(7p-1)\omega_x\omega_y^2-2(p+2)\omega_x\omega_z^2+(p+1)\omega_y^3-2(p-2)\omega_y\omega_z^2}{\Delta},$$

$$\frac{m_2^{(2)}}{m_p} = p\frac{\Gamma^4+2i\Gamma^3\omega_z+\Gamma^2\left(4\omega_x^2+4\omega_y^2+\omega_z^2\right)+i\Gamma\omega_z\left(5\omega_x^2+5\omega_y^2+2\omega_z^2\right)+3\left(\omega_x+i\omega_y\right)^2\left(\omega_x^2-\omega_y^2\right)}{\Delta}$$
$$+\frac{(\omega_x+i\omega_y)^2\left(\Gamma^2+3i\Gamma\omega_z+\omega_x^2+\omega_y^2-2\omega_z^2\right)}{\Delta}, \tag{A1}$$

where $\Delta = \Gamma^4+5\Gamma^2(\omega_x^2+\omega_y^2+\omega_z^2)+4(\omega_x^2+\omega_y^2+\omega_z^2)^2$ and p is the degree of polarization.

APPENDIX B: JACOBI-ANGER EXPANSIONS

The Jacobi-Anger expansions used in this article are [50]

$$\exp(iz\,\sin\theta) = \sum_{n=-\infty}^{\infty} J_n(z)\exp(in\theta),$$

$$\sin(z\,\sin\theta) = 2\sum_{n=0}^{\infty} J_{2n+1}(z)\sin(2n+1)\theta,$$

$$\cos(z\,\sin\theta) = J_0(z)+2\sum_{n=1}^{\infty} J_{2n}(z)\cos 2n\theta. \tag{B1}$$

[1] H.-C. Koch, G. Bison, Z. D. Grujić, W. Heil, M. Kasprzak, P. Knowles, A. Kraft, A. Pazgalev, A. Schnabel, J. Voigt *et al.*, Eur. Phys. J. D **69**, 202 (2015).

[2] T. Jager, J.-M. Léger, F. Bertrand, I. Fratter, and J.-C. Lalaurie, *2010 IEEE Sensors* (IEEE, New York, 2010), pp. 2392–2395.

[3] V. Shifrin, P. G. Park, C. Kim, V. Khorev, and C. H. Choi, IEEE Trans. Instrum. Meas. **46**, 97 (1997).

[4] V. Shah, G. Vasilakis, and M. V. Romalis, Phys. Rev. Lett. **104**, 013601 (2010).

[5] G. Vasilakis, H. Shen, K. Jensen, M. Balabas, D. Salart, B. Chen, and E. S. Polzik, Nature Physics **11**, 389 (2015).

[6] A. Weis, G. Bison, N. Castagna, S. Cook, A. Hofer, M. Kasprzak, P. Knowles, and J.-L. Schenker, *17th International Conference on Biomagnetism Advances in Biomagnetism – Biomag2010* (Springer, Berlin, Heidelberg, 2010), pp. 58–61.

[7] R. Wyllie, M. Kauer, R. T. Wakai, and T. G. Walker, Opt. Lett. **37**, 2247 (2012).

[8] H. Xia, A. Ben-Amar Baranga, D. Hoffman, and M. V. Romalis, Appl. Phys. Lett. **89**, 211104 (2006).

[9] C. Gemmel, W. Heil, S. Karpuk, K. Lenz, C. Ludwig, Y. Sobolev, K. Tullney, M. Burghoff, W. Kilian, S. Knappe-Grüneberg *et al.*, Eur. Phys. J. D **57**, 303 (2010).

[10] W. Heil, C. Gemmel, S. Karpuk, Y. Sobolev, K. Tullney, F. Allmendinger, U. Schmidt, M. Burghoff, W. Kilian, S. Knappe-Grüneberg *et al.*, Ann. Phys. (N.Y.) **525**, 539 (2013).

[11] S. Afach, C. A. Baker, G. Ban, G. Bison, K. Bodek, M. Burghoff, Z. Chowdhuri, M. Daum, M. Fertl, B. Franke *et al.*, Phys. Lett. B **739**, 128 (2014).

[12] A. Weis, G. Bison, and Z. D. Grujić, in *High Sensitivity Magnetometers*, edited by A. Grosz, M. J. Haji-Sheikh, and S. C. Mukhopadhyay (Springer, New York, 2017).

[13] J. Dupont-Roc, Rev. Phys. Appl. **5**, 853 (1970).

[14] C. Cohen-Tannoudji, J. Dupont-Roc, S. Haroche, and F. Laloë, Rev. Phys. Appl. **5**, 95 (1970).

[15] C. Cohen-Tannoudji, J. Dupont-Roc, S. Haroche, and F. Laloë, Rev. Phys. Appl. **5**, 102 (1970).

[16] J. Dupont-Roc, J. Phys. **32**, 135 (1971).

[17] R. Wyllie, Ph.D. thesis, University of Wisconsin–Madison, 2012.

[18] C. Cohen-Tannoudji and J. Dupont-Roc, Phys. Rev. A **5**, 968 (1972).

[19] C. Guttin, J. M. Leger, and F. Stoeckel, J. Phys. IV **4**, C4-655 (1994).

[20] J. Rutkowski, W. Fourcault, F. Bertrand, U. Rossini, S. Gétin, S. Le Calvez, T. Jager, E. Herth, C. Gorecki, M. Le Prado *et al.*, Sens. Actuators, A **216**, 386 (2014).

[21] A. Weis, G. Bison, and A. S. Pazgalev, Phys. Rev. A **74**, 033401 (2006).

[22] E. Breschi and A. Weis, Phys. Rev. A **86**, 053427 (2012).

[23] D. D. McGregor, Rev. Sci. Instrum. **58**, 1067 (1987).

[24] J.-M. Leger, F. Bertrand, T. Jager, M. Le Prado, I. Fratter, and J.-C. Lalaurie, Procedia Chemistry **1**, 634 (2009).
[25] R. E. Slocum, Phys. Rev. Lett. **29**, 1642 (1972).
[26] R. E. Slocum and B. Marton, IEEE Trans. Magn. **9**, 221 (1973).
[27] S. Morales, M.-C. Corsi, W. Fourcault, F. Bertrand, G. Cauffet, C. Gobbo, F. Alcouffe, F. Lenouvel, M. L. Prado, F. Berger *et al.*, Phys. Med. Biol. **62**, 7267 (2017).
[28] E. Labyt, M.-C. Corsi, W. Fourcault, A. Palacios-Laloy, F. Bertrand, F. Lenouvel, G. Cauffet, M. Le Prado, F. Berger, and S. Morales, IEEE Trans. Med. Imaging, doi: 10.1109/TMI.2018.2856367.
[29] F. D. Colegrove and P. A. Franken, Phys. Rev. **119**, 680 (1960).
[30] S. S. Hodgman, R. G. Dall, L. J. Byron, K. G. H. Baldwin, S. J. Buckman, and A. G. Truscott, Phys. Rev. Lett. **103**, 053002 (2009).
[31] A. V. Phelps and J. P. Molnar, Phys. Rev. **89**, 1202 (1953).
[32] J. W. Shon and M. J. Kushner, J. Appl. Phys. **75**, 1883 (1994).
[33] Y. Sakiyama and D. B. Graves, J. Phys. D **39**, 3644 (2006).
[34] S. Rauf and M. J. Kushner, J. Appl. Phys. **85**, 3460 (1999).
[35] G. D. Cates, S. R. Schaefer, and W. Happer, Phys. Rev. A **37**, 2877 (1988).
[36] W. Happer, Y.-Y. Jau, and T. Walker, *Optically Pumped Atoms* (Wiley, New York, 2010).
[37] D. Budker, W. Gawlik, D. F. Kimball, S. M. Rochester, V. V. Yashchuk, and A. Weis, Rev. Mod. Phys. **74**, 1153 (2002).
[38] S. I. Kanorsky, A. Weis, J. Wurster, and T. W. Hänsch, Phys. Rev. A **47**, 1220 (1993).
[39] A. Weis, J. Wurster, and S. I. Kanorsky, JOSA B **10**, 716 (1993).
[40] Y. Shi, T. Scholtes, Z. D. Grujić, V. Lebedev, V. Dolgovskiy, and A. Weis, Phys. Rev. A **97**, 013419 (2018).
[41] A. Omont, Prog. Quantum Electron. **5**, 69 (1977).
[42] C. Cohen-Tannoudji and J. Dupont-Roc, Opt. Commun. **1**, 184 (1969).
[43] F. Laloë, M. Leduc, and P. Minguzzi, J. Phys. **30**, 277 (1969).
[44] M. Auzinsh, D. Budker, and S. Rochester, *Optically Polarized Atoms: Understanding Light-atom Interactions* (Oxford University Press, Oxford, 2010).
[45] C. Landré, C. Cohen-Tannoudji, J. Dupont-Roc, and S. Haroche, J. Phys. **31**, 971 (1970).
[46] C. Cohen-Tannoudji, J. Phys. Colloq. **32**, C5a-11 (1971).
[47] S. Haroche, Ph.D. thesis, Univ. Paris VI, 1971.
[48] N. Polonsky and C. Cohen-Tannoudji, J. Phys. **26**, 409 (1965).
[49] W. Happer, Phys. Rev. B **1**, 2203 (1970).
[50] *Handbook of Mathematical Functions: with Formulas, Graphs, and Mathematical Tables*, 9th ed., edited by M. Abramowitz and I. A. Stegun (Dover Publications, New York, 1965).
[51] G. D. Cates, D. J. White, T.-R. Chien, S. R. Schaefer, and W. Happer, Phys. Rev. A **38**, 5092 (1988).